

PI²-Controller Applied to a Piezoelectric Nanopositioner Using Conditional Integrators and Optimal Tuning

Arnfinn Aas Eielsen* Mernout Burger*
Jan Tommy Gravdahl* Kristin Y. Pettersen*

* *Department of Engineering Cybernetics, Norwegian University of Science and Technology, 7491 Trondheim, Norway*
(e-mail: {arnfinn.aas.eielsen,mernout.burger,
jan.tommy.gravdahl,kristin.ytterstad.pettersen}@itk.ntnu.no).

Abstract: For tracking control of nanopositioning stages using piezoelectric actuators, controllers with integral action can be employed to robustly track a reference in the presence of hysteresis, creep, and plant parametric uncertainties. In any practical configuration of instrumentation for this application, saturations will be present. Thus, a controller with integral action is prone to windup, which typically cause large transients and long settling times, and will in general degrade performance and potentially damage equipment. In this paper it is demonstrated that conditional integrators provides a very accessible and convenient framework for introducing anti-windup for any order integral controller, and the effectiveness is verified experimentally. Also, the influence reconstruction and anti-aliasing filters have on the stability limits for PI and PI² controllers is investigated, and a novel tuning procedure is proposed in order to obtain the best performance for the overall system. It is demonstrated experimentally that optimal tuning can damp resonances and increase bandwidth.

Keywords: Eigenvalue placement, integral control, lowpass filters, numerical analysis, optimal control, output regulation, tracking.

1. INTRODUCTION

A typical system for high precision positioning, found in systems for scanning probe microscopy, optical alignment, and data storage (see e.g. Devasia et al. [2007] for a survey), consists of several elements in addition to the actual mechanical positioning stage. It includes high-resolution position sensors, low-noise amplifiers, a fast computer or micro-controller to implement the control algorithm, fast and high-resolution digital-to-analog and analog-to-digital converters to interface sensors and actuators, as well as reconstruction and anti-aliasing filters to reduce aliasing phenomena and quantization noise. These elements will typically be limited in usable input and output range, as well as exhibit low-pass characteristic behavior. Signals can therefore saturate, and amplitude attenuation and phase lag will occur as a signal propagates through a cascaded interconnection of components.

Tracking reference trajectories for nanopositioning systems is often performed using integral or double integral controllers, due to plant parametric uncertainties and the presence of disturbances such as hysteresis and creep. For high precision positioning, signals will often be scaled to reduce noise and to maximize resolution. For example; it is common to adjust the amplification of the signal from the digital-to-analog converter (DAC) such that the maximum output of the DAC corresponds to the maximum mechanical deflection desired, utilizing the full range of the DAC and thus maximizing the resolution. This leaves a small margin before saturation, and will make a controller with integral action prone to windup in the presence of disturbances such as measurement bias and variable con-

trol gain. To retain some level of performance and avoid large transients, an integral anti-windup scheme should be used. Among the large assortment of anti-windup schemes (see e.g. Rundqwist [1991] for a survey), the conditional integrator scheme of Seshagiri and Khalil [2005] is used in the following. It is straight forward to analyze and implement for integral controllers of any order. The use of conditional integrators is demonstrated experimentally to practically eliminate any adverse effects due to windup.

It is to be expected that any low-pass characteristic element in the signal chain will influence the stability and performance of a closed-loop system. When applying a discrete controller to a continuous system, anti-aliasing and reconstruction filters must be present to attenuate frequency content above the Nyquist-frequency to avoid aliasing, as well as to reduce quantization noise. Low-pass filters applied for such a task are often easily parameterized and adjustable with respect to the cut-off frequency. The filters dynamics will often also be dominant compared to other elements in the signal chain. Thus, taking these filters into account when analyzing and tuning the closed-loop system could therefore provide a very accessible performance improvement. It is demonstrated that for the experimental system used, the optimal tuning increases the bandwidth with more than an order of magnitude.

2. SYSTEM DESCRIPTION AND MODELING

We consider a system consisting of a mechanical positioning stage, anti-aliasing and reconstruction filters, as well as a feedback controller and a feed-forward filter. A diagram of this system is shown in Fig. 1. As the amplifier and sensor used in the experimental set-up have very fast

dynamics, they have been mostly neglected in the following analysis. We note that all signals in the diagram have limited range in practice, and can saturate.

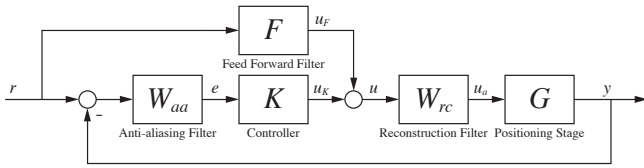


Fig. 1. System Diagram.

2.1 Positioning Stage

A second order system should be a very good approximation to the displacement dynamics of a well designed nanopositioning stage. Given the model for a second order system (A.2), which is

$$\ddot{x} + 2\zeta\omega_0\dot{x} + \omega_0^2x = \beta_0u, \quad (1)$$

we can find estimates of the parameter values for the damping coefficient ζ , natural undamped frequency ω_0 , and the control gain β_0 , using frequency response data. Identified parameters for the nanopositioner used in the experiments are presented in Tab. 1.

Table 1. Identified parameters for the positioning stage, using the parameterization in (1).

Parameter	Value	Unit
ζ	0.0139	1
ω_0	$2\pi \times 781$	1/s
β_0	2.36×10^6	$1/s^2 \cdot \mu\text{m}/V$

As can be seen, $\zeta \ll 1/\sqrt{2}$, which indicates that the positioning stage has a very large resonance peak at $\omega_p \approx \omega_0$.

2.2 Anti-Aliasing and Reconstruction Filters

For convenience, the anti-aliasing and reconstruction filters used were identical, i.e.

$$W_{aa}(s) = W_{rc}(s).$$

In the experimental setup, they were second-order low-pass Butterworth filters. The filter dynamics can therefore also be described by (1). Given the parameterization of (1), the parameter values that render a second-order low-pass Butterworth filter response for the model are given in Tab. 2.

Table 2. Second order Butterworth filter parameters, using the parameterization in (1).

Parameter	Value	Unit
ζ	$1/\sqrt{2}$	1
ω_0	$\omega_c = 2\pi f_c$	1/s
β_0	ω_c^2	$1/s^2$

The filter has one tunable parameter, the cut-off frequency $\omega_c = 2\pi f_c$. In the experimental system, a dSPACE 1103 hardware-in-the-loop system was used to implement the control system. This system can reliably be used with a sampling period of $\tau_s = 20 \mu\text{s}$. To mitigate aliasing and quantization effects, the cut-off frequency for both the anti-aliasing and the reconstruction filter should be lower than the Nyquist-frequency $f_c \leq f_n = 0.5/\tau_s = 25 \text{ kHz}$ [Proakis and Manolakis, 1995].

2.3 Feed-Forward Filter

Considering Fig. 1, the ideal feed-forward filter from the reference r to the voltage applied to the reconstruction filter u , would be to use the inverse of the dynamical models for the reconstruction filter and the positioning stage, i.e.

$$u_F(s) = W_{rc}^{-1}(s) \cdot G^{-1}(s) \cdot r(s).$$

The parameter values for the parameters $\{\zeta, \omega_0, \beta_0\}$ in the actual implementation of the reconstruction filter are constant, and therefore using the inverse model with constant parameters is very accurate. The parameter values for the positioning stage do, on the other hand, change quite noticeably with temperature, offset voltage, load, displacement range, as well as due to depolarization of the piezoelectric actuator and perhaps other unknown factors.

The experimental setup provided only position measurement. Generating the time derivatives of the position measurement using standard techniques, such as numerical differentiation, high-gain observers, or using the Luenberger observer, introduced noise and/or large estimation errors. Standard implementations of on-line parameter identification schemes, such as the gradient or the least-squares method, did not provide good parameter estimates when trying to estimate the parameters $\{\zeta, \omega_0, \beta_0\}$ for the positioning stage.

We therefore opted to approximate the relationship between applied voltage, u_a , and the measured deflection, y , as a static gain:

$$y(s) = G(s)u_a(s) \approx K_d u_a(s)$$

The coefficient $K_d = \beta_0/\omega_0^2$ was estimated on-line using least-squares. To accommodate for the reconstruction filter W_{rc} and the amplifier gain K_a , the feed-forward filter F used was chosen to be

$$u_F = \frac{1}{K_d K_a \omega_c^2} \left(\ddot{r} + \sqrt{2}\omega_c \dot{r} + \omega_c^2 r \right), \quad (2)$$

where ω_c is the cut-off frequency for the filter. Using this formulation, the reference signal r should be piecewise continuous and sufficiently smooth.

2.4 Controller

The control signal applied to the system is a linear combination of the feed-forward filter u_F and the feedback controller u_K , i.e. $u = u_F + u_K$. The feed-forward filter then achieves coarse positioning, and the feedback controller should then reduce the residual error.

Triangle-wave trajectories are common when applying nanopositioning devices in scanning probe microscopy, thus the chosen controller was geared towards providing good tracking performance when using such references. As noted in Section 2.3, the instrumentation only provide position measurement, and it was difficult to obtain good parameter estimates on-line. Generating time derivatives from the output and an inverting feed forward yielded fairly poor results. Therefore, in order to robustly track a triangle-wave reference signal with reasonable accuracy, a PI²-controller was employed. As the triangle-wave reference consists of a series of ramps, the double integral action should provide exponential convergence of the output to the flanks of the reference signal. The controller was implemented using conditional integrators in order to add anti-windup in the presence of saturations. The anti-aliasing

and reconstruction filters were included in the analysis, and both filters and controller were tuned optimally to reduce resonance and increase bandwidth.

The details of the controller derivation will be presented in Section 3, and the stability and tuning analysis is presented in Section 4.

3. PI²-CONTROLLER WITH ANTI-WINDUP USING CONDITIONAL INTEGRATORS

Adding anti-windup to a controller with integral action will in general retain some level of performance and avoid large transients if saturations occur. In this section we show how conditional integrators [Seshagiri and Khalil, 2005] can be used to achieve anti-windup for the chosen PI² controller. The conditional integrator framework is seen to provide a very straight forward implementation and analysis, and the scheme can easily be extended to controllers with integral action of any order. The conditional integrator control scheme is based on continuous sliding mode control with integral action, and is designed to only provide integral action if the value for the so-called *sliding mode variable* is below some given threshold.

We define the sliding mode variable as

$$\varsigma = k_0\sigma_1 + k_1\sigma_2 + k_2\varepsilon, \quad (3)$$

where the error ε is defined as $\varepsilon = v - \rho$, and ρ and v are the reference signal r and the output y filtered by the anti-aliasing filter, that is,

$$\rho(s) = W_{aa}(s)r(s) \quad \text{and} \quad v(s) = W_{aa}(s)y(s).$$

The signals $\sigma_{1,2}$ are generated by the system

$$\begin{aligned} \dot{\sigma}_1 &= \sigma_2 \\ \dot{\sigma}_2 &= -k_0\sigma_1 - k_1\sigma_2 + \mu \text{sat}(\varsigma/\mu). \end{aligned} \quad (4)$$

Using (3) and (4), and if the sign of the control gain of the plant is positive, the control signal is produced by

$$u_K = -\beta_K \text{sat}(\varsigma/\mu), \quad (5)$$

thus $u_K \in [-\beta_K, \beta_K]$.

In the above expressions, the saturation function $\text{sat}(\cdot)$ is used. This function is defined as

$$\text{sat}(z) = \begin{cases} z & \text{if } |z| \leq 1 \\ \text{sgn}(z) & \text{if } |z| > 1, \end{cases}$$

where $\text{sgn}(z)$ denotes the sign of the quantity z . The parameter $\mu > 0$ is used to set the threshold of saturation for the sliding mode variable ς , and the parameter $\beta_K > 0$ determines the maximum value of the control signal.

By inspecting the equations for the controller, (3), (4), and (5), (4) can be manipulated into the form

$$\begin{aligned} \dot{\sigma}_1 &= \sigma_2 \\ \dot{\sigma}_2 &= k_2\varepsilon - k_0\sigma_1 - k_1\sigma_2 - k_2\varepsilon + \mu \text{sat}(\varsigma/\mu) \\ &= k_2\varepsilon - \varsigma + \mu \text{sat}(\varsigma/\mu) \\ &= k_2\varepsilon + \frac{\mu}{\beta_K}(u_K - u_K^*), \end{aligned} \quad (6)$$

where we have introduced u_K^* , which is (5) without saturation, i.e.

$$u_K^* = -\beta_K(\varsigma/\mu). \quad (7)$$

Saturation occurs when the absolute value for the sliding mode variable ς is above the value of μ . The controller therefore has two modes of operation; the unsaturated mode, when $|\varsigma| \leq \mu$, and the saturated mode, when $|\varsigma| > \mu$.

When $|\varsigma| \leq \mu$, we have the unsaturated case, and thus $u_K = u_K^*$. The system represented in (4) or (6) becomes

$$\begin{aligned} \dot{\sigma}_1 &= \sigma_2 \\ \dot{\sigma}_2 &= k_2\varepsilon, \end{aligned}$$

and we see that the signals $\sigma_{1,2}$ are time integrals of the error ε , scaled by the constant k_2 .

The control signal (5) is in this case given as

$$u_K = k_p e + k_i \int_{t_0}^t e \, d\tau + k_{ii} \int_{t_0}^t \int_{t_0}^{\tau} e \, d\tau' \, d\tau \quad (8)$$

where $e = -\varepsilon$,

$$k_p = \frac{\beta_K}{\mu} k_2, \quad k_i = \frac{\beta_K}{\mu} k_1 k_2, \quad \text{and} \quad k_{ii} = \frac{\beta_K}{\mu} k_0 k_2,$$

which we recognize as a PI²-controller.

In the unsaturated mode, stability and tracking performance can then be determined by analyzing the closed-loop system using (8) with controller gains k_p , k_i , and k_{ii} . For a set of control gains, $\{k_p, k_i, k_{ii}\}$, the parameters for (3) and (4) are found as

$$k_2 = \frac{\mu}{\beta_K} k_p, \quad k_1 = \frac{k_i}{k_p}, \quad \text{and} \quad k_0 = \frac{k_{ii}}{k_p}.$$

When $|\varsigma| > \mu$, the saturated case occurs, and $u_K \neq u_K^*$. The system (4), or (6), becomes

$$\begin{aligned} \dot{\sigma}_1 &= \sigma_2 \\ \dot{\sigma}_2 &= -k_0\sigma_1 - k_1\sigma_2 + \mu \text{sgn}(\varsigma), \end{aligned} \quad (9)$$

and the control output (5) becomes the constant

$$u_K = -\beta_K \text{sgn}(\varsigma). \quad (10)$$

Inspecting (9), we see that if the characteristic equation

$$\lambda^2 + k_1\lambda + k_0 = 0$$

is Hurwitz, the state vector (σ_1, σ_2) converges exponentially to $(\mu/k_0, 0)$ or $(-\mu/k_0, 0)$, depending on the sign of the sliding mode variable ς , and this behavior prevents windup in the controller. By the Routh-Hurwitz criterion, the characteristic equation will be Hurwitz if $k_{0,1} > 0$.

4. STABILITY ANALYSIS

In the above analysis of the anti-windup scheme, we see that the control signal u_K can either be the constant (10) in the saturated case, or generated by (8) for the unsaturated case. The system will therefore switch between a mode where feedback is applied, and a mode where it is driven in open-loop. The behavior of the system in the saturated case is then determined by the open-loop dynamics. The overall system as depicted in Fig. 1 consists of a series of stable sub-systems. For the open-loop system

$$G_{ol}(s) = W_{rc}(s) \cdot G(s) \cdot W_{aa}(s)$$

we note that in the absence of feedback, the location of the eigenvalues remains unchanged.

In the unsaturated case, the closed-loop system will be of order eight if we only consider the filter dynamics and use the second-order approximation to the mechanical dynamics. Analytic analysis is therefore cumbersome and does not provide good insight into the stability conditions and performance. To analyze the closed-loop behavior, we first investigate the closed-loop stability considering only the mechanical dynamics $G(s)$, and derive some rules of thumb for choosing the controller gains k_p and k_i , since the obtained stability limits correspond well with what can be obtained using graphical techniques. Next, we provide some numerical analysis in order to determine the closed-loop stability and performance of the overall system.

4.1 Proportional Gain Margin

When applying a proportional controller

$$u = k_p e$$

to the second order system (1), in the ideal case with perfect sensors and actuators, it is easy to verify that the closed-loop system has an unlimited stability margin, that is, k_p can be chosen arbitrarily large. In the presence of phase-lag this margin is severely limited. Considering e.g. sensor dynamics in the form of the first-order low-pass filter with cut-off frequency $\omega_c = 2\pi f_c$

$$\dot{x} = -\omega_c x + \omega_c u = -2\pi f_c x + 2\pi f_c u \quad (11)$$

in cascade with (1) we find, using the Routh-Hurwitz criterion, that the margin k_p^* for the combined system is given as

$$k_p < \frac{2\zeta\omega_0(\omega_0^2 + 2\zeta\omega_0\omega_c + \omega_c^2)}{\omega_c\beta_0} = k_p^*. \quad (12)$$

With parameter values from Tab. 1, and considering the specifications for a fast state-of-the-art capacitive probe from ADE Technologies (ADE 6810), which is well described by (11) with $f_c = 100$ kHz, we find that $k_p \lesssim 35$. Adding more low-pass characteristic elements degrades the margin even more, until the allowable control gain is too low to produce noticeable effects in the sensitivity function, $N(s) = \frac{e}{r}(s)$.

4.2 Integral Gain Margin

Considering an integral controller

$$u = k_i \int_{t_0}^t e \, d\tau$$

applied to (1), the stability margin k_i^* , again using Routh-Hurwitz criterion, can be found to be

$$k_i < \frac{2\zeta\omega_0^3}{\beta_0} = k_i^*. \quad (13)$$

Given a lightly damped system, $0 < \zeta \ll 1/\sqrt{2}$, knowing the resonance frequency ω_p and the amplitude response at resonance $|G(j\omega_p)|$, we can express this, by using (A.4) and (A.7), as

$$k_i < \frac{\omega_p}{|G(j\omega_p)|} < \kappa \cdot \frac{\omega_p}{|G(j\omega_p)|} = k_i^*$$

where $\kappa^{-1} = \sqrt{1 - \zeta^2} \cdot \sqrt{1 - 2\zeta^2} < 1$, which corresponds well with the result found in Fleming et al. [2010].

We note that adding proportional action to the above controller, the effective stiffness of the system increases. The product $\zeta\omega_0^3$ will therefore be larger, and thus the margin becomes larger.

4.3 Interim Summary

Summarizing the above analysis, it is clear that when the damping coefficient ζ is small, the proportional gain is severely limited due to low-pass characteristic elements in the signal chain. The integral gain is also limited by the damping coefficient, and a good estimate of the gain limit can be found knowing only the resonance frequency and the magnitude of the amplitude response at resonance. It can be therefore conjectured that attenuating the resonance peak (or increasing the resonance frequency) improves both gain margins.

4.4 Effects of Low-Pass Filters in the Signal Chain

For a more thorough investigation of the stability margins and closed-loop bandwidth for the system, the reconstruction and anti-aliasing filters were added to the model. Setting the control gains to $k_p = 0.1$, $k_i = k_i^*$, and $k_{ii} = 0$, i.e. using a PI-controller with control gains on the margin of stability, the eigenvalue loci of the closed-loop system was generated by varying the cut-off frequency $\omega_c = 2\pi f_c$ of the reconstruction and anti-aliasing filters. These eigenvalue loci are presented in Fig. 2.

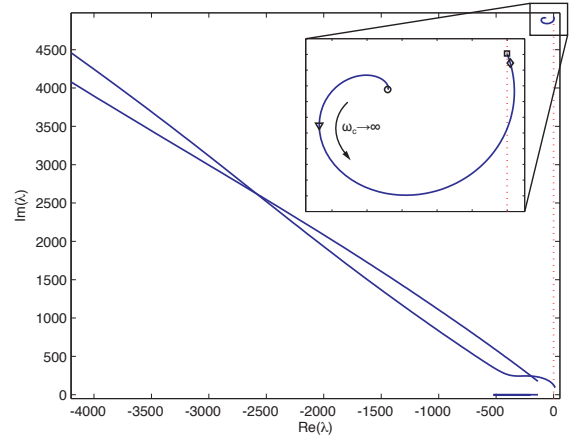


Fig. 2. Eigenvalue loci for the closed-loop system as a function of the filter cut-off frequency ω_c . The loci are symmetric about the real axis. In the detail from the upper-right corner, $\omega_c = 0$ is indicated by a circle, $\omega_c = \omega_o$ a triangle, $\omega_c = \omega_n$ a diamond shape, and $\omega_c = \infty$ a square.

As can be seen, using filters with a cut-off frequency equal to the Nyquist frequency, $2\pi f_c = \omega_c = \omega_n = 2\pi f_n$, where $f_n = 25$ kHz, the system is unstable. The plot indicates however, that reducing the cut-off frequency for the filters, all eigenvalues can be moved further into the left-half plane. Minimizing the maximum value of the real part of the eigenvalues for the closed-loop system as a function of the cut-off frequency f_c resulted in

$$\arg \min_{f_c \in \mathbb{R}^+} [\arg \max_{\text{Re}(\lambda) \in \mathbb{R}^-} [\det(A(f_c) - \lambda I) = 0]] \approx 850 \text{ Hz}$$

where $A(f_c)$ is a state matrix realization for the closed-loop system for a given f_c . Thus, setting $\omega_c = \omega_o = 2\pi f_o$, $f_o = 850$ Hz, will produce the fastest modes for this system.

By inspecting Fig. 2, it is evident that by using the computed optimal value for the cut-off frequency, the stability margins for the closed-loop system will be larger. This should allow for a larger closed-loop bandwidth. The new stability margin was found numerically to be about $14.8 \cdot k_i^*$. To produce the flattest possible response for the complementary sensitivity function, an optimal value of k_i was found as

$$\arg \min_{k_i \in [0, 14.8 \cdot k_i^*]} \|1 - |M(j\omega, \alpha)|\|^2 \approx 7.5 \cdot k_i^*$$

Using the optimal cut-off frequency and the above optimal integral gain should produce the flattest frequency response when using a PI-controller, and it yielded a gain margin of $\Delta K = 5.93$ dB and a phase margin of $\Psi = 57.2^\circ$.

Adding double integral action, it was difficult to find a good optimality criterion, as a large double integral gain

would introduce peaking, i.e. a new resonance peak in the closed-loop system. In a similar vein as above, the objective function

$$J(k_i, k_{ii}) = \|1 - |M(j\omega, \alpha, k_{ii})|\|^2 \quad (14)$$

was evaluated numerically to determine what combination of gains, k_i and k_{ii} , would produce the flattest frequency response. The result is presented in Fig. 3. As can be seen, the objective function is convex along the direction for k_i , but increasing in the direction for k_{ii} . Using $k_i = 8.4 \cdot k_i^*$ and $k_{ii} = 5.7 \times 10^6$ rendered $\Delta K = 4.36$ dB and $\Psi = 29.3^\circ$.

Using a cut-off frequency equal to the Nyquist-frequency, (14) did not produce a convex behavior for gains within the stability margins, thus the optimal value for k_i would be on the stability limit, and the optimal value for k_{ii} would be zero. Thus, the gains were chosen to match the gain margin above, while avoiding excessive peaking. Using $k_i = 0.60 \cdot k_i^*$ and $k_{ii} = 10^5$ yielded $\Delta K = 4.15$ dB and $\Psi = 44.5^\circ$.

The resulting frequency responses are displayed in Fig. 4. As can be seen, the optimal tuning increases the bandwidth with more than an order of magnitude.

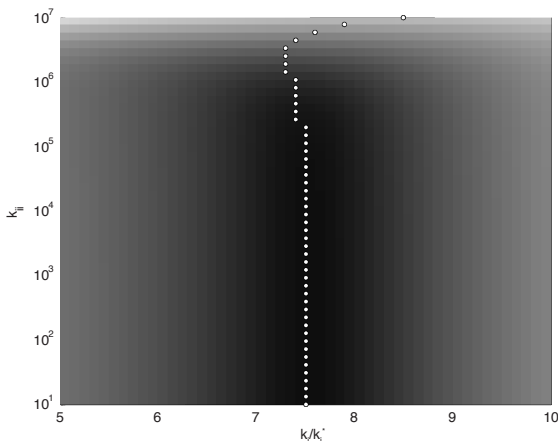


Fig. 3. Numerical evaluation of the objective function (14), using $f_c = 850$ Hz. Dark areas represents low values, and light areas represents high values. Minimal values occurring while tracing the abscissa have been indicated by dots.

5. EXPERIMENTAL RESULTS

To validate the results, four experiments were performed. Tracking a reference signal, $r \in C^2$, results were recorded when using the nominal tuning, the optimal tuning, as well as when using anti-windup and with anti-windup turned off.

The experimental set-up consisted of a dSPACE DS1103 hardware-in-the-loop board, a ADE 6810 capacitive gauge and ADE 6501 capacitive probe from ADE Technologies, a Piezodrive PDL200 voltage amplifier, a long-range serial-kinematic nanopositioner from easyLab, as well as two SIM 965 programmable filters from Stanford Research Systems.

The results while tracking a reference with a fundamental frequency of 50 Hz and an amplitude of $1 \mu\text{m}$, using optimal and nominal tuning are presented in Figs. 5 and 6. The increased bandwidth makes it possible to reduce the root-mean-square error from 67 nm when using the nominal tuning, to 14 nm when using the optimal tuning. Inspection of the spectral content of the error signals in

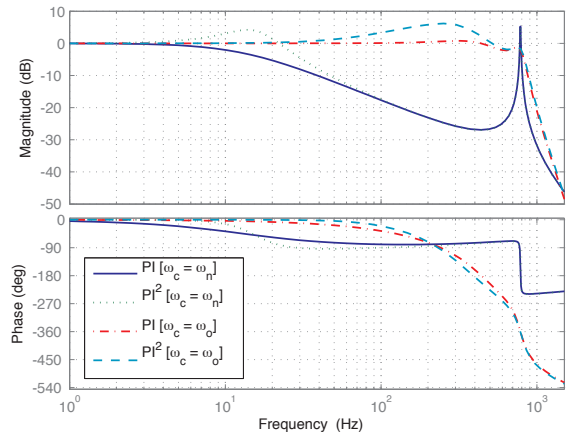


Fig. 4. Amplitude and phase response for the complementary sensitivity function $M(s) = \frac{y}{r}(s)$, using PI and PI²-controllers. The filter cut-off frequency was set to the Nyquist frequency, $f_n = 25$ kHz, or the optimal frequency $f_o = 850$ Hz.

Fig. 6, reveals that the power of the 781 Hz component in the signal, due to the prominent resonance in the system, was reduced from -63 dB/Hz to -75 dB/Hz.

The effectiveness of the anti-windup scheme is demonstrated in Fig. 7. The reference signal has a fundamental frequency of 5 Hz and an amplitude of $1 \mu\text{m}$. Here, saturation in control signal was introduced using a SIM 964 analog limiter from Stanford Research Systems on the output from the digital-to-analog converter. As can be seen, without anti-windup there are large transients and long settling times, which are practically eliminated when using the anti-windup scheme.

6. CONCLUSIONS

For a PI²-controller applied to a nanopositioner, two very accessible techniques has been demonstrated to improve the performance when tracking a reference trajectory. An anti-windup scheme based on conditional integrators practically eliminated large transients and long settling times that occurred when signals in the system saturated. Also, by optimally tuning the reconstruction and anti-aliasing filters, that always are present when implementing a controller in discrete time, bandwidth of the closed-loop system was increased by more than an order of magnitude,

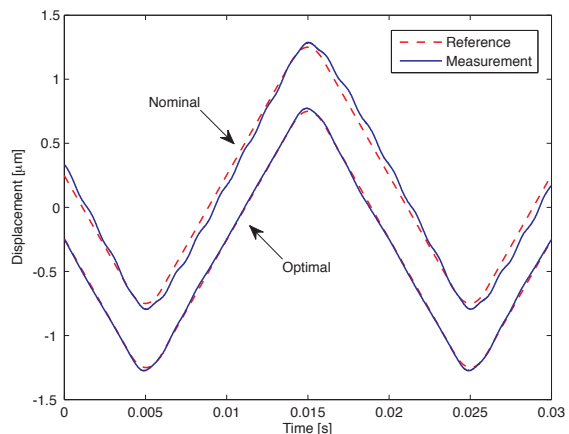


Fig. 5. Optimal tuning vs. nominal tuning. $\pm 1 \mu\text{m}$ displacement with 50 Hz fundamental frequency.

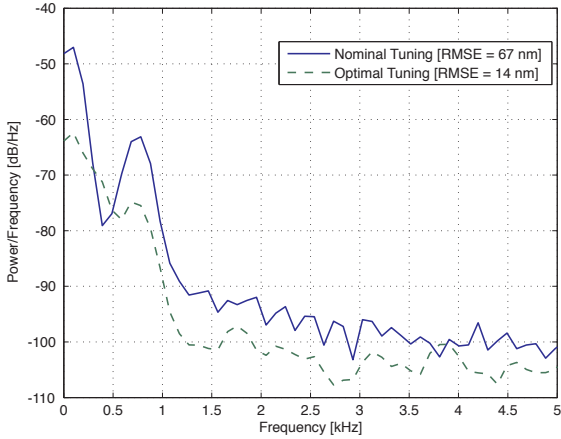


Fig. 6. Power spectral density estimates of the error signals.

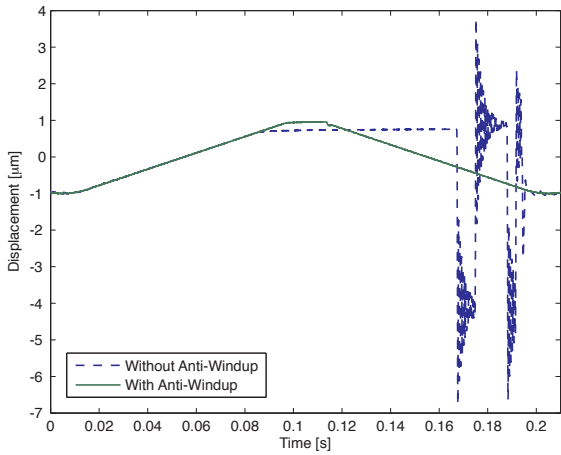


Fig. 7. Anti-windup effectiveness.

resulting in smaller tracking errors and attenuation of the mechanical resonance present in the nanopositioner.

It is interesting to note that by utilizing the reconstruction and anti-aliasing filters in this fashion, one obtains very similar results as when applying integral resonance control [Fleming et al., 2009], but with the added advantage of using equipment already present in the signal chain.

ACKNOWLEDGEMENTS

Supported by the Norwegian Research Council and the Norwegian University of Science and Technology. The authors would like to thank Christian Holden for valuable feedback and comments, as well as Dr. Kam K. Leang for providing the positioning stage, and Dr. Andrew Fleming for providing the amplifier used.

REFERENCES

- S Devasia, E Eleftheriou, and SOR Moheimani. A survey of control issues in nanopositioning. *Control Systems Technology, IEEE Transactions on*, 15(5):802–823, 2007.
- AJ Fleming, S Aphale, and SOR Moheimani. A new robust damping and tracking controller for spm positioning stages. In *Proceedings of the American Control Conference, St. Louis, MO*, pages 289–294, 2009.
- AJ Fleming, BJ Kenton, and KK Leang. Bridging the gap between conventional and video-speed scanning probe microscopes. *Ultramicroscopy*, 110(9):1205–1214, 2010.

JG Proakis and DG Manolakis. *Digital Signal Processing*. Prentice Hall, Inc., 3rd edition, 1995.

L Rundqwist. *Anti-Reset Windup for PID Controllers*. PhD thesis, Lund Institute of Technology, 1991.

S Seshagiri and HK Khalil. Robust output feedback regulation of minimum-phase nonlinear systems using conditional integrators. *Automatica*, 41:43–54, 2005.

Appendix A. SOME FACTS ABOUT SECOND-ORDER SYSTEMS

The dynamics of a non-autonomous mass-spring-damper system is described by the second-order system

$$m\ddot{x} + c\dot{x} + kx = \beta u(t) \quad (\text{A.1})$$

where k is the spring constant, c is the damping coefficient, m is the mass, and β is the control gain. For this system, the undamped natural (angular) frequency ω_0 and damping ratio ζ are defined as

$$\omega_0 = \sqrt{\frac{k}{m}} \quad \text{and} \quad \zeta = \frac{c}{2\sqrt{mk}},$$

thus, with $\beta_0 = \frac{\beta}{m}$, (A.1) can be written

$$\ddot{x} + 2\zeta\omega_0\dot{x} + \omega_0^2x = \beta_0 u(t). \quad (\text{A.2})$$

For (A.2) we find the damped natural frequency as

$$\omega_d = \omega_0\sqrt{1 - \zeta^2}. \quad (\text{A.3})$$

When we have $u(t) = 0$, the system is autonomous. The damped natural frequency is the frequency an autonomous underdamped system ($\zeta < 1$) will oscillate with given a set of initial values $(x_0, \dot{x}_0) \neq (0, 0)$.

The resonant frequency for (A.2) is

$$\omega_p = \omega_0\sqrt{1 - 2\zeta^2}. \quad (\text{A.4})$$

The resonant frequency is the frequency at which the non-autonomous system will have the maximum amplitude response. The amplitude response will only have a peak when $0 \leq \zeta < 1/\sqrt{2}$.

The Laplace transform of (A.2) is

$$G(s) = \frac{\beta_0}{s^2 + 2\zeta\omega_0s + \omega_0^2}. \quad (\text{A.5})$$

The amplitude response is found from the Fourier transform ($s = j\omega$) as

$$|G(j\omega)| = \frac{\beta_0}{\sqrt{(\omega_0^2 - \omega^2)^2 + (2\zeta\omega_0\omega)^2}} = \frac{\beta_0}{\sqrt{\Delta(\omega)}}. \quad (\text{A.6})$$

Differentiating (A.6) with respect to the angular frequency ω we find

$$\frac{d}{d\omega} |G(j\omega)| = -\frac{1}{2}\Delta(\omega)^{-3/2}\Delta'(\omega)$$

where

$$\Delta'(\omega) = 4\omega(\omega^2 - \omega_0^2)(1 - 2\zeta^2),$$

thus it should be straight forward to verify that

$$\arg \max_{\omega \in \mathbb{R}^+} |G(j\omega)| = \omega_p$$

if $0 < \zeta < 1/\sqrt{2}$, and if $\zeta \geq 1/\sqrt{2}$

$$\arg \max_{\omega \in \mathbb{R}^+} |G(j\omega)| = 0.$$

For $0 < \zeta < 1/\sqrt{2}$ the amplitude response at $\omega = \omega_p$ is

$$|G(j\omega_p)| = \frac{\beta_0}{2\zeta\omega_0^2\sqrt{1 - \zeta^2}}. \quad (\text{A.7})$$